

Clues on the Physical Origin of the Fundamental Plane from Self-consistent Hydrodynamical Simulations

J. Oñorbe¹, R. Domínguez-Tenreiro¹, A. Sáiz^{1,2}, A. Serna³, H. Artal¹

jose.onnorbe@uam.es, rosa.dominguez@uam.es, alex@astro.phys.sc.chula.ac.th,
arturo.serna@umh.es, hector.artal@uam.es

ABSTRACT

We report on a study of the parameters characterizing the mass and velocity distributions of two samples of relaxed elliptical-like-objects (ELOs) identified, at $z = 0$, in a set of self-consistent hydrodynamical simulations operating in the context of a concordance cosmological model. Star formation (SF) has been implemented in the simulations in the framework of the turbulent sequential scenario through a phenomenological parameterization that takes into account stellar physics processes implicitly through the values of a threshold gas density and an efficiency parameter. Each ELO sample is characterized by the values these parameters take. We have found that the (logarithms of the) ELO stellar masses, projected half-stellar mass radii, and stellar central l.o.s. velocity dispersions define *dynamical* Fundamental Planes (FPs). Zero-points depend on the particular values that the SF parameters take, while slopes do not change. The ELO samples have been found to show systematic trends with the mass scale in both, the relative content and the relative distributions of the baryonic and the dark mass ELO components. The physical origin of these trends lies in the systematic decrease, with increasing ELO mass, of the relative dissipation experienced by the baryonic mass component along ELO mass assembly, resulting into a tilt of the dynamical FP relative to the virial plane. ELOs also show kinematical segregation, but it does not appreciably change with the mass scale. We have found that the dynamical FPs shown by the two ELO samples are consistent with that shown by the SDSS elliptical sample in the same variables, with no further need for any relevant contribution from stellar population effects to explain the observed tilt. These effects could, however, have contributed to the scatter of the observed FP, as the dynamical FPs have been found to be thinner than the observed one. The results we report on hint, for the first time, to a possible way to understand the tilt of the observed FP in a cosmological context.

Subject headings: dark matter: galaxies: elliptical and lenticular, cD - galaxies: evolution - galaxies: formation - galaxies: fundamental parameters - hydrodynamics - methods: n-body simulations

1. INTRODUCTION

The 3-parameter space of the observed effective radius, R_e^{light} , the mean surface brightness within that radius, $\langle I^{\text{light}} \rangle_e$, and the central line-of-sight (los) velocity dispersion, $\sigma_{\text{los},0}$, of early-type galaxies is not homogeneously populated. These galaxies define a plane on this space, known as the Fundamental Plane (FP, Djorgovski & Davis 1987; Dressler et al. 1987a; Faber et al. 1987; Kormendy & Djorgovski 1989) defined by:

$$\log_{10} R_e^{\text{light}} = a \log_{10} \sigma_{\text{los},0} + b \log_{10} \langle I^{\text{light}} \rangle_e + c. \quad (1)$$

A new standard of reference for nearby elliptical galaxies is provided by the Sloan digital sky survey (SDSS, see York et al. 2000) sample of early-type galaxies (see Bernardi et al. 2003a, 2003b, 2003c for the Early Data Release), containing to date 9000 morphologically selected ellipticals from different environments, a number larger than the number of ellipticals in all the previously analyzed samples. The values of the FP coefficients from this sample are $a \simeq 1.5$, similar in the four SDSS bands, $b \simeq -0.77$, and $c \simeq -8.7$ (see their exact values in Bernardi et al. 2003c, Table 2) with a small scatter. These SDSS results confirm previous ones, either in the optical (Lucey, Bower & Ellis 1991; de Carvalho & Djorgovski 1992; Bender, Burstein & Faber 1992; Jorgensen et al. 1993; Prugniel & Simien 1996; Jorgensen et al. 1996) or in the near-IR wavelengths (Recillas-Cruz et al. 1990, 1991; Pahre, Djorgovski & de Carvalho 1995; Mobasher et al. 1999), even if the published values of a show larger values in the K -band than at shorter wavelengths (see, for example, Pahre, de Carvalho & Djorgovski 1998).

The existence of the FP and its small scatter has the important implication that it provides us with a strong constraint when studying elliptical galaxy formation and evolution (Bender, Burstein & Faber 1993; Guzmán, Lucey & Bower 1993; Renzini & Ciotti 1993). The physical origin of the FP is not yet clear, but it must be a consequence of the physical processes responsible for galaxy assembly. These processes built up early type galaxies as dynamically hot systems whose configuration in phase space are close to equilibrium. Taking an elliptical galaxy as a system in equilibrium, a mass scale M_{FP} can be estimated from the observable R_e^{light} , $\langle I^{\text{light}} \rangle_e$ and $\sigma_{\text{los},0}$ parameters through the expression:

$$M_{\text{FP}} = 3c_M \sigma_{\text{los},0}^2 R_e^{\text{light}} / G, \quad (2)$$

¹Dpt. Física Teórica C-XI, Universidad Autónoma de Madrid, E-28049 Cantoblanco, Madrid, Spain; ² Current address: Dept. of Physics, Mahidol University, Bangkok 10400, Thailand; ³ Dpt. Física y A.C., Universidad Miguel Hernández, E-03206 Elche, Alicante, Spain

where G is the gravitational constant and c_M is a mass structure coefficient. The total luminosity of the galaxy is given by the expression $L = 2\pi \langle I^{\text{light}} \rangle_e (R_e^{\text{light}})^2$. As Faber et al. (1987) first pointed out, the virial theorem $M_{\text{vir}} = c_F (\sigma_3^{\text{tot}})^2 r_e^{\text{tot}} / G$, with σ_3^{tot} the average 3-dimensional velocity dispersion of the whole elliptical, including both dark and baryonic matter, r_e^{tot} the dynamical half-radius or radius enclosing half the total mass of the system, and c_F a form factor of order unity, would imply

$$R_e^{\text{light}} = \frac{3c_M^{\text{vir}} L \sigma_{\text{los},0}^2 \langle I^{\text{light}} \rangle_e^{-1}}{2\pi G M_{\text{vir}}} \quad (3)$$

where c_M^{vir} is defined by Eq. (2) when $M_{\text{FP}} = M_{\text{vir}}$, that is

$$c_M^{\text{vir}} = \frac{G M_{\text{vir}}}{3\sigma_{\text{los},0}^2 R_e^{\text{light}}}, \quad (4)$$

or

$$c_M^{\text{vir}} = c_F c_v c_r \quad (5)$$

with $c_v = (\sigma_3^{\text{tot}})^2 / 3\sigma_{\text{los},0}^2$ and $c_r = r_e^{\text{tot}} / R_e^{\text{light}}$. Assuming that both the quantities c_M^{vir} and the dynamical mass-to-light ratios, M_{vir}/L , are independent of mass, the scaling relation $R_e^{\text{light}} \propto \sigma_{\text{los},0}^2 \langle I^{\text{light}} \rangle_e^{-1}$ would then hold. However, this predicted scaling law is inconsistent with those found observationally ($a \neq 2, b \neq -1$), i.e., the FP is tilted relative to the virial relation, implying that at least some of the assumptions made to derive it is incorrect.

Different authors interpret the tilt of the FP relative to the virial relation as caused by different misassumptions that we comment briefly (note that we can write $M_{\text{vir}}/L = M^{\text{star}}/L \times M_{\text{vir}}/M^{\text{star}}$, where M^{star} is the stellar mass of the elliptical galaxy): i) A first possibility is that the tilt is due to systematic changes of stellar age and metallicity with galaxy mass, or, even, to changes of the slope of the stellar initial mass function (hereafter, IMF) with galaxy mass, resulting in systematic changes in the *stellar*-mass-to-light ratios, M^{star}/L , with mass or luminosity (Zepf & Silk 1996; Pahre et al. 1998; Mobasher et al. 1999). But these effects could explain at most only \sim one third of the $\beta \neq 0$ value in the *B*-band (Tinsley 1978; Dressler et al. 1987; Prugniel & Simien 1996; see also Renzini & Ciotti 1993; Trujillo, Burkert & Bell 2004). Furthermore, early-type galaxies in the SDSS have been found to have roughly constant stellar-mass-to-light ratios (Kauffmann et al. 2003a, 2003b). Anyhow, the presence of a tilt in the *K*-band FP, where population effects are no important, indicates that it is very difficult that the tilt is caused by stellar physics processes alone, as Bender et al. (1992), Renzini & Ciotti (1993), Guzmán et al. (1993), Pahre et al. (1998), among other authors, have suggested. ii) A second possibility is that M_{vir}/L changes systematically with the mass scale because the total dark-to-visible mass ratio, $M_{\text{vir}}/M^{\text{star}}$ changes (see, for example, Renzini & Ciotti 1993; Pahre et al. 1998;

Ciotti, Lanzoni & Renzini 1996; Padmanabhan et al. 2004). Otherwise, a dependence of c_M^{vir} on the mass scale could be caused by systematic differences in iii), the dark versus bright matter spatial distribution, which could be measured through systematic variations of the c_r coefficients with mass, iv), the kinematical segregation, the rotational support and/or velocity dispersion anisotropy in the stellar component (dynamical non-homology), measurable through the c_V coefficients, and, v), systematic geometrical effects, measurable through the c_F , c_r or c_V coefficients. Taking into account these effects in the FP tilt demands modelling the galaxy mass and velocity three-dimensional distributions and comparing the outputs with high quality data. Bender et al. (1992) considered effects iii) and iv); Ciotti et al. (1996) explore ii) - iv) and conclude that an systematic increase in the dark matter content with mass, or differences in its distribution, as well as a dependence of the Sérsic (1968) shape parameter for the luminosity profiles with mass, may by themselves formally produce the tilt; Padmanabhan et al. (2004) find evidence of effect ii) in SDSS data. Other authors have also shown that allowing for broken homology, either dynamical (Busarello et al. 1997), in the luminosity profiles (Trujillo et al. 2004), or both (Prugniel & Simien 1997; Graham & Colless 1997; Pahre et al. 1998), brings the observed FP closer to the virial plane.

One important source of ambiguity in observational data analysis comes from the impossibility to get accurate measurements of the elliptical three-dimensional mass distributions (either dark, stellar or gaseous) and velocity distributions. Analytical models give very interesting insights into these distributions as well as the physical processes causing them, but are somewhat limited by symmetry considerations and other necessary simplifying hypotheses. Self-consistent gravo-hydrodynamical simulations are a very convenient tool to work out this problem, as they *directly* provide with complete 6-dimensional phase-space information on each constituent particle sampling a given galaxy-like object formed in the simulation, that is, they give directly the mass and velocity distributions of dark matter, gas and stars of each object. This phase space information allows us to test whether or not the c_M^{vir} (that is, the c_F , c_V and c_r) coefficients, as well as the $M_{\text{vir}}/M^{\text{star}}$ ratios, do or do not systematically depend on the mass scale. This is the issue addressed in this Letter, where we analyze whether the dependence is such that the tilt and the scatter of the observed FP can be explained in terms of the regularities in the structural and dynamical properties of ELOs formed in self-consistent hydrodynamical simulations.

2. The Dynamical Fundamental Plane of Simulated Objects

In a self-consistent numerical approach initial conditions are set at high z as a Monte-carlo realization of the field of primordial fluctuations in a given cosmological model; then

the evolution of these fluctuations is numerically followed up to $z = 0$ by means of a computing code that solves the N-body plus hydrodynamical evolution equations. We have run ten simulations in the framework of a flat Λ CDM cosmological model, with $\Omega_\Lambda = 0.65$, $\Omega_{\text{baryon}} = 0.06$, $\sigma_8 = 1.18$ and $h = 0.65$. The code used in our simulations is DEVA (Serna, Domínguez-Tenreiro, & Sáiz 2003). In this code, particular attention has been paid to the implementation of conservation laws (energy; entropy, taking into account the ∇h terms; angular momentum). Star formation (SF) has been implemented in the code in the framework of the turbulent sequential scenario (Elmegreen 2002) through a phenomenological parameterization, that transforms cold locally-collapsing gas, denser than a threshold density, ρ_{thres} , into stars with a timescale given by the empirical Kennicutt-Schmidt law (Kennicutt 1998), with an average star formation efficiency at the scales resolved by the code c_* ; possible feedback effects are implicitly taken into account through the values of the SF parameters. In any run, 64^3 dark matter and 64^3 baryon particles, with a mass of 1.29×10^8 and $2.67 \times 10^7 M_\odot$, respectively, have been used to homogeneously sample the density field in a periodic box of 10 Mpc side. We refer the reader to Serna et al. 2003 and to Sáiz, Domínguez-Tenreiro, & Serna 2004 for further details on the simulation technique and SF implementation in the code. Five out of the ten simulations (the SF-A type simulations) share the SF parameters ($\rho_{\text{thres}} = 6 \times 10^{-25}$ gr cm $^{-3}$, $c_* = 0.3$) and differ in the seed used to build up the initial conditions. To test the role of SF parameterization, the same initial conditions have been run with different SF parameters ($\rho_{\text{thres}} = 1.8 \times 10^{-24}$ gr cm $^{-3}$, $c_* = 0.1$) making SF more difficult, contributing another set of five simulations (hereafter, the SF-B type simulations). Galaxy-like objects of different morphologies appear in the simulations. ELOs have been identified as those objects having a prominent dynamically relaxed stellar spheroidal component, with no disks and very low cold gas content. This stellar component has typical sizes of no more than $\sim 10 - 40$ kpc and it is embedded in a halo of dark matter typically ten times larger in size. ELOs have also an extended corona of hot diffuse gas. It turns out that 26 (17) out of the more massive objects formed in SF-A (SF-B) type simulations fulfil this condition, giving the hereafter termed SF-A and SF-B ELO samples. Note that due to their respective SF implementations, galaxy-like objects formed in SF-A type simulations tend to be of earlier type than their counterparts formed in SF-B type simulations; this is why the ELO number in SF-A sample is higher than in SF-B sample. Moreover, gas has had more time to lose energy along SF-B type ELO assembly than in their SF-A type counterparts, and, consequently, the former have smaller sizes than the latter.

Following the discussion in §1, two mass scales have been measured on ELOs: the virial mass M_{vir} , or total mass of the ELO at its halo scale (we adopt the fitting formula of Bryan & Norman, 1998, for the spherical overdensity at virialization), and the stellar mass at the ELO scale, $M_{\text{bo}}^{\text{star}}$. Concerning length scales, the relevant ones are: i), at the halo scale: the

virial radii, r_{vir} and the half-total mass radii, $r_{\text{e,h}}^{\text{tot}}$, enclosing $M_{\text{vir}}/2$; and ii), at the ELO scale, the stellar half-mass radii, $r_{\text{e,bo}}^{\text{star}}$, defined as those radii enclosing half the $M_{\text{bo}}^{\text{star}}$ mass, and the projected stellar half-mass radii, $R_{\text{e,bo}}^{\text{star}}$, measured onto the projected mass distribution. The total (including baryons and dark matter) mean square velocity within r_{vir} , $\sigma_{3,\text{h}}^{\text{tot}}$, as well as the mean square stellar and central stellar² l.o.s velocity dispersions, $\sigma_{3,\text{bo}}^{\text{star}}$ and $\sigma_{\text{los},0}^{\text{star}}$, respectively, have also been measured on ELOs. Note that the scales entering the virial relation are $r_{\text{e,h}}^{\text{tot}}$ and $\sigma_{3,\text{h}}^{\text{tot}}$ and that they are not observationally available. Assuming that the projected stellar *mass* distribution, $\Sigma_{\text{star}}(R)$, can be taken as a measure of the surface *brightness* profile, then $\langle \Sigma_{\text{star}} \rangle_e = c \langle I^{\text{light}} \rangle_e$, with c a constant, and $R_{\text{e,bo}}^{\text{star}} \simeq R_{\text{e}}^{\text{light}}$ and we can look for a fundamental plane (hereafter, the dynamical FP) in the 3-space of the structural and dynamical parameters $R_{\text{e,bo}}^{\text{star}}$, $\langle \Sigma_{\text{star}} \rangle_e$ and $\sigma_{\text{los},0}^{\text{star}}$, directly provided by the hydrodynamical simulations. To make this analysis as clear as possible, we transform to a κ -like orthogonal coordinate system, the dynamical κ_i^{D} system, $i=1,2,3$, similar to that introduced by Bender, Burstein & Faber (1992), but using $R_{\text{e,bo}}^{\text{star}}$ instead of $R_{\text{e}}^{\text{light}}$ and $\langle \Sigma_{\text{star}} \rangle_e$ instead of $\langle I^{\text{light}} \rangle_e$, and, consequently, free of age, metallicity or IMF effects. The κ^{D} and κ coordinates are related by the expressions: $\kappa_1 \simeq \kappa_1^{\text{D}}$, $\kappa_2 \simeq \kappa_2^{\text{D}} - \sqrt{6}/3 \log M_{\text{bo}}^{\text{star}}/L$ and $\kappa_3 \simeq \kappa_3^{\text{D}} + \sqrt{3}/3 \log M_{\text{bo}}^{\text{star}}/L$. We discuss the tilt and the scatter of the dynamical FP separately. We first address the tilt issue. We use at this stage for the $R_{\text{e,bo}}^{\text{star}}$ and $\sigma_{\text{los},0}^{\text{star}}$ variables the averages over three orthogonal l.o.s. projections, to minimize the scatter in the plots caused by projection effects.

Figure 1 plots the κ_3^{D} versus κ_1^{D} (top) and κ_2^{D} versus κ_1^{D} (bottom) diagrams for ELOs in the SF-A (filled symbols) and SF-B (open symbols) samples. We also drew the 2σ concentration ellipses in the respective variables, as well as its major and minor axes, for the SDSS early-type galaxy sample in the z band as analyzed by Bernardi et al. 2003b, 2003c³. We recall that the ellipse major axis corresponds to the orthogonal mean square regression line for the two variables in the Figure (for further details see Sáiz et al. 2004). The most outstanding feature of Figure 1 (upper panel) is the good scaling behaviour of κ_3^{D} versus κ_1^{D} , with a very low scatter (see the slopes M_1 in Table 1; note that the slopes for the SF-A and SF-B samples are consistent within their errors while the zero-points depend on the SF parameterization through the ELO sizes). The values of the slopes in Table 1 mean that systematic variations of the structural and dynamical properties of ELOs with the mass scale cause, by themselves, a tilt of the dynamical FP relative to the virial relation. Another interesting feature of Figure 1 is that it shows that most of the values of the κ_i^{D} coefficients

²Recall that the empirical l.o.s velocity dispersion, $\sigma_{\text{los},0}$, is measured through *stellar spectra*

³The constant stellar-mass-to-light ratios allow us to write the covariance matrix using the $E \equiv \log M_{\text{bo}}^{\text{star}}$ variable instead of absolute magnitude or the logarithm of the luminosity L

are within the 2σ concentration ellipses in both plots for ELOs formed in SF-A type simulations, with a slightly worse agreement for ELOs in the SF-B sample. This means that ELOs have counterparts in the real world (Sáiz et al. 2004). It is also worth mentioning that these results are stable against slight changes in the values of the Ω_Λ , Ω_{baryon} or h parameters; for example, we have tested that using their preferred WMAP values shows results negligibly different to those plotted in Figure 1.

To deepen into the causes of the tilt, we have calculated the slope β_{vir} of the $M_{\text{vir}}/M_{\text{bo}}^{\text{star}} \propto (M_{\text{bo}}^{\text{star}})^{\beta_{\text{vir}}}$ scaling relation for ELOs in the SF-A and SF-B samples (Table 1). We got $\beta_{\text{vir}} > 0$, indicating that the mass fraction of stars bound to the ELOs (or, more generically, cold baryons) relative to total mass within r_{vir} decreases with the mass scale (as suggested by Renzini & Ciotti 1993 and Pahre et al. 1998). We have also found that the $c_{\text{M}}^{\text{vir}}$ coefficients show a mass dependence that can be parametrized as a scaling relation $c_{\text{M}}^{\text{vir}} \propto (M_{\text{bo}}^{\text{star}})^{\beta_{\text{M}}}$ (broken homology, see Table 1). As discussed in §1, different possible sources for homology breaking exist. To dilucidate which of them are relevant, we first note that the c_{V} and c_{r} coefficients can be written as: $c_{\text{V}} = c_{\text{VD}} \times c_{\text{VPC}}$, with $c_{\text{VD}} \equiv (\sigma_{3,\text{h}}^{\text{tot}}/\sigma_{3,\text{bo}}^{\text{star}})^2$ and $c_{\text{VPC}} \equiv (\sigma_{3,\text{bo}}^{\text{star}})^2/3(\sigma_{\text{los},0}^{\text{star}})^2$ and $c_{\text{r}} = c_{\text{rD}} \times c_{\text{rP}}$ with $c_{\text{rD}} \equiv r_{\text{e,h}}^{\text{tot}}/r_{\text{e,bo}}^{\text{star}}$ and $c_{\text{rP}} \equiv r_{\text{e,h}}^{\text{star}}/R_{\text{e,bo}}^{\text{star}}$. This gives $c_{\text{M}}^{\text{vir}} = c_{\text{F}}c_{\text{VD}}c_{\text{VPC}}c_{\text{rD}}c_{\text{rP}}$, where the c_{VD} and c_{rD} factors measure the kinematical and spatial segregations between dark and stellar matter, respectively, while c_{VPC} and c_{rP} measure projection and other geometrical effects in the stellar mass and velocity distributions. Writting $c_i \propto (M_{\text{bo}}^{\text{star}})^{\beta_i}$, with $i = \text{F, VD, VPC, rD, rP}$, we get $\beta_{\text{M}} = \beta_{\text{F}} + \beta_{\text{VD}} + \beta_{\text{VPC}} + \beta_{\text{rD}} + \beta_{\text{rP}}$ when the β_i slopes are calculated through direct fits. These β_i slopes are given in Table 1, as well as their 95 % confidence intervals both for the SF-A and SF-B samples. We see that, irrespective of the SF parameterization, the main contribution to the homology breaking comes from the c_{rD} coefficients (see Guzmán et al. 1993), while β_{F} and β_{VD} have values consistent with c_{F} and c_{VD} being independent of the ELO mass scale, c_{rP} and c_{VPC} show a very mild mass dependence in the SF-A sample and none in the SF-B sample.

We now turn to consider the scatter of the dynamical FP for the ELO samples and compare it with the scatter of the FP for the SDSS elliptical sample, calculated as the square root of the smallest eigenvalue of the 3×3 covariance matrix in the E (or $\log L$), V and R variables (Saglia et al. 2001). As Figure 1 (top) suggests, when projection effects are circumvented by taking averages over different directions, the resulting three dimensional orthogonal scatter for ELOs is smaller than for SDSS ellipticals ($\sigma_{\text{EVR}} = 0.0164$ and $\sigma_{\text{EVR}} = 0.0167$ for the SF-A and SF-B samples, respectively, to be compared with $\sigma_{\text{LVR}} = 0.0489$ for the SDSS in the $\log L, V$ and R variables). To estimate the contribution of projection effects to the observed scatter, we have calculated the orthogonal scatter for ELOs when no averages over projection directions for the $R_{\text{e,bo}}^{\text{star}}$ and $\sigma_{\text{los},0}^{\text{star}}$ variables are made. The scatter ($\sigma_{\text{EVR}} = 0.0238$ and $\sigma_{\text{EVR}} = 0.0214$ for the SF-A and SF-B samples) increases, but it is still

lower than observed. This indicates that a contribution from stellar population effects is needed to explain the scatter of the observed FP, as suggested by different authors (see, for example, Pahre et al. 1998; Trujillo et al. 2004).

To sum up, the ELO samples have been found to show systematic trends with the mass scale in both, the relative content and the relative distributions of the baryonic and the dark mass ELO components. These trends do not significantly depend on the star formation parameterization and they are due to a systematic decrease, with increasing ELO mass, of the relative amount of dissipation experienced by the baryonic mass component along ELO formation, a possibility that Bender et al. (1992), Guzmán et al. (1993), and Ciotti et al. (1996) had suggested. These trends cause a tilt of the virial plane in such a way that there is no further need of any relevant contribution from stellar population effects to explain the observed tilt. The scatter of the observed FP, however, probably requires a contribution from such stellar effects.

This work was partially supported by the MCyT and MEyD (Spain) through grants AYA-0973, AYA-07468-C03-02 and AYA-07468-C03-03 from the PNAyA. We thank the Centro de Computación Científica (UAM, Spain) for computing facilities. AS thanks FEDER financial support from UE.

REFERENCES

- Bender, R., Burstein, D., & Faber, S.M. 1992, ApJ, 399, 462;
1993, ApJ, 411, 153
- Bernardi, M., et al. 2003a, AJ, 125, 1817; 2003b, AJ, 125, 1849; 2003c, AJ, 125, 1866
- Bryan, G.L., & Norman, M.L. 1998, ApJ, 495, 80
- Busarello, G., Capaccioli, M., Capozziello, S., Longo, G., & Puddu, E 1997, A&A, 320, 415
- Ciotti, L., Lanzoni, B., & Renzini, A. 1996, MNRAS, 282, 1
- de Carvalho, R.R., & Djorgovski, S. 1992, ApJ, 389, L49
- Djorgovski, S., & Davis, M. 1987, ApJ, 313, 59
- Dressler, A., Lynden-Bell, D., Burstein, D., Davies, R.L., Faber, S.M., Terlevich, R., & Wegner, G. 1987, ApJ, 313, 42
- Elmegreen, B.G. 2002, ApJ, 577, 206
- Faber, S.F., Dressler, A., Davies, R.L., Burstein, D., Lynden-Bell, D., Terlevich, R., & Wegner, G. 1987, in *Nearly Normal Galaxies: From the Planck Time to the Present*, ed. S.M. Faber (New York: Springer), 175
- Graham, A., & Colless, M. 1997, MNRAS, 287, 221
- Guzmán, R., Lucey, J., & Bower, R.G. 1993, MNRAS, 265, 731
- Jorgensen, I., Franx, M., & Kjaergaard, P. 1993, ApJ, 411, 34;
1996, MNRAS, 280, 167
- Kauffmann, G., et al., 2003a, MNRAS, 341, 33
- Kauffmann, G., et al., 2003b, MNRAS, 341, 54
- Kennicutt, R. 1998, ApJ, 498, 541
- Kormendy, J., & Djorgovski, S. 1989, ARA&A, 27, 235
- Lucey, J.R., Bower, R.J., & Ellis, R.S. 1991, MNRAS, 249, 755
- Mobasher, B., Guzmán, R., Aragón-Salamanca, A., & Zepf, S. 1999, MNRAS, 304, 225
- Padmanabhan, N., et al. 2004, New A., 9, 329

- Pahre, M.A., de Carvalho, R.R., & Djorgovski, S.G. 1998, *AJ*, 116, 1606
- Pahre, M.A., Djorgovski, S.G., & de Carvalho, R.R. 1995, *ApJ*, 453, L17
- Prugniel, Ph., & Simien, F. 1996, *A&A*, 309, 749; 1997, *A&A*, 321, 111
- Recillas-Cruz et al. 1990, *A&A*, 229, 64; 1991, *A&A*, 249, 312
- Renzini, A., & Ciotti, L. 1993, *ApJ*, 416, L49
- Saglia, R. P., Colless, M., Burstein, D., Davies, R.L., McMahan, R.K., & Wegner, G. 2001, *MNRAS*, 324, 389
- Sáiz, A., Domínguez-Tenreiro, R., & Serna, A. 2004, *ApJ*, 601, L131
- Serna, A., Domínguez-Tenreiro, R., & Sáiz, A. 2003, *ApJ*, 597, 878
- Sérsic, J.L. 1968, *Atlas de galaxias australes* (Córdoba, Argentina: Observatorio Astronómico)
- Tinsley, B.M. 1978, *ApJ*, 222, 14
- Trujillo, I., Burkert, A., & Bell, E.F. 2004, *ApJ*, 600, L39
- York D.G., et al., 2000, *AJ*, 120, 1579
- Zepf, S. & Silk, J. 1996, *ApJ*, 466, 114

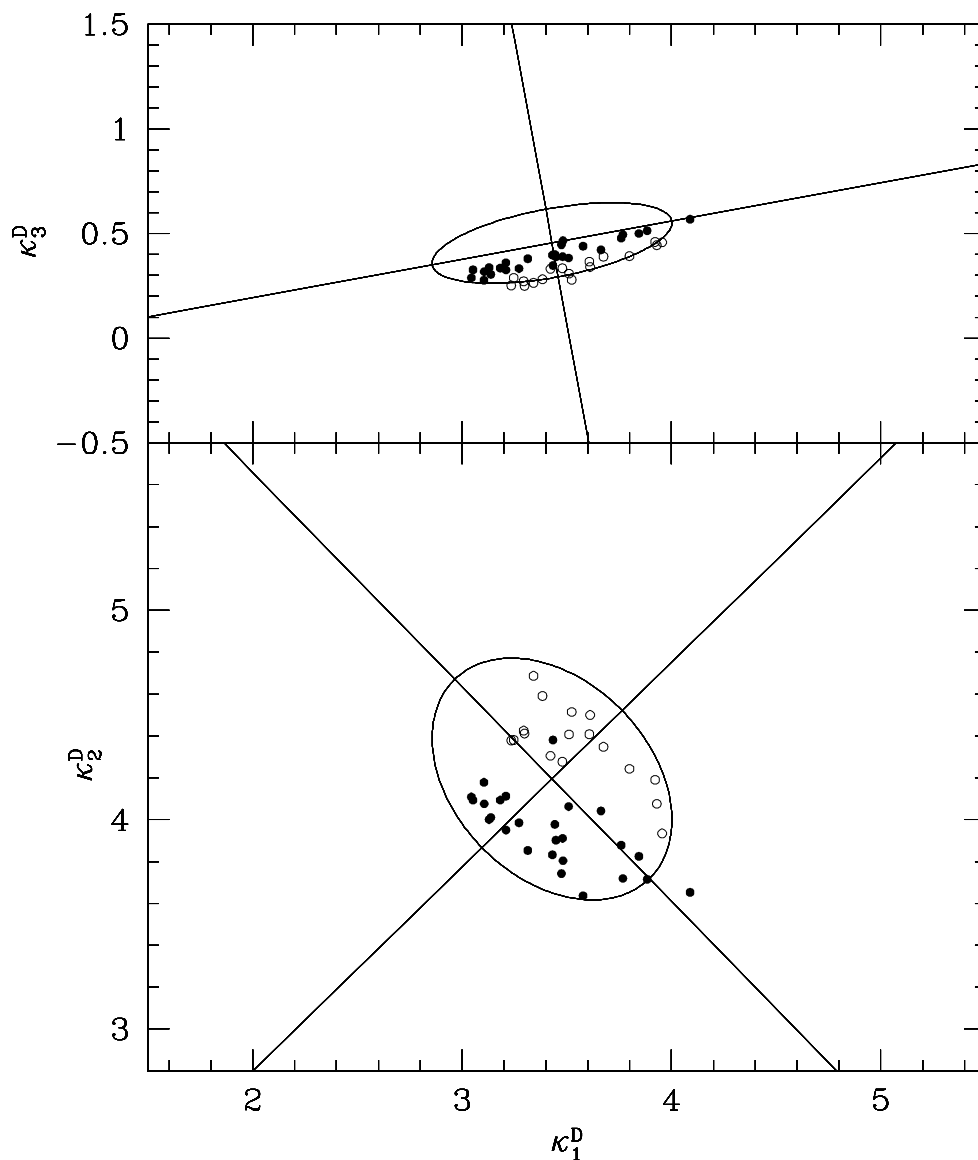


Fig. 1.— Edge-on projection (top panel) and nearly-face-on projection (bottom panel) of the dynamical FP of ELOs in the κ^D variables (filled circles: SF-A sample; open circles: SF-B sample). We also draw the respective concentration ellipses (with their major and minor axes) for the SDSS early-type galaxy sample from Bernardi et al. (2003b) in the z -band. See text for more details

Table 1:

	SF-A		SF-B	
M_1	0.256	± 0.035	0.281	± 0.048
β_{vir}	0.221	± 0.083	0.237	± 0.158
β_{M}	-0.204	± 0.116	-0.247	± 0.189
β_{F}	0.025	± 0.048	0.022	± 0.081
β_{VD}	0.021	± 0.041	0.076	± 0.075
β_{VPC}	-0.044	± 0.029	-0.044	± 0.093
β_{rD}	-0.225	± 0.127	-0.316	± 0.199
β_{rP}	0.019	± 0.009	0.016	± 0.017

Column 2: the slopes of the $\kappa_3^{\text{D}} = M_1 \kappa_1^{\text{D}} + M_0$ relation (direct fits); the slopes of the $M_{\text{vir}}/M_{\text{bo}}^{\text{star}}$ and $c_i \propto (M_{\text{bo}}^{\text{star}})^{\beta_i}$ scaling relations for the the SF-A sample, calculated in log – log plots through direct fits. Column 3: their respective 95% confidence intervals. Columns 4 and 5: same as columns 2 and 3 for the SF-B sample.